DOI: 10.26599/FSHW.2025.9250847

Contents lists available at SciOpen

Food Science and Human Wellness

journal homepage: https://www.sciopen.com/journal/2097-0765

China Food Publishing Co.

Eriodictyol Attenuates Doxorubicin-Induced Cardiotoxicity by Inhibiting Ferroptosis through Targeting FABP4

Chunmeng Qin[ab], Qinglong Liu[a], Xiangru Zheng[c], Feng Lv[a], Mei Sun[a], Dan Du[a], Songqing Liu[a]*, Wenjun Li [a]*

[a] *Department of Pharmacy, The Third Affiliated Hospital of Chongqing Medical University, Chongqing, China*

[b] *College of Pharmacy, Chongqing Medical University, Chongqing, China*

[c] *Department of Hepatobiliary and Pancreatic Surgery, The Third Affiliated Hospital of Chongqing Medical University, Chongqing, China*

ABSTRACT: Doxorubicin (DOX), while an effective chemotherapeutic agent, is often associated with severe cardiotoxicity, significantly limiting its clinical use. Recent studies suggest that ferroptosis, a regulated form of cell death, plays a critical role in DOX-induced cardiac injury. Eriodictyol (ERD), a naturally occurring flavonoid compound abundantly found in citrus fruits and certain traditional Chinese herbs, has demonstrated promising cardioprotective properties; however, whether ERD can ameliorate DOX-induced cardiac injury and the underlying mechanisms of its action remain unexplored. In this study, a model of DOX-induced cardiotoxicity was established using C57BL/6 mice and H9c2 cells to investigate the cardioprotective effects of ERD. ERD treatment significantly reduced ferroptosis, alleviated mitochondrial damage and improved cardiac function. Further studies revealed that ERD may target fatty acid-binding protein 4 (FABP4) to exert its effects. Functional experiments confirmed that FABP4 knockdown impaired the protective effects of ERD, highlighting its essential role in ferroptosis inhibition. These findings indicate that ERD protects against DOX-induced cardiotoxicity primarily through the modulation of FABP4 and ferroptosis pathways, offering a potential therapeutic strategy for mitigating DOX-related adverse effects.

Keywords Eriodictyol; Ferroptosis; Doxorubicin; Cardiotoxicity; Fatty acid binding protein 4.

1. Introduction

Doxorubicin (DOX) is a broad-spectrum anthracycline antibiotic used clinically for various tumours, including malignant lymphoma, breast cancer, and sarcoma [1, 2]. However, doxorubicin-induced cardiotoxicity (DIC), characterized by irreversible ventricular dysfunction and intractable heart failure, significantly limits its clinical application. Studies indicate a high incidence rate of DIC, reaching 26% when the cumulative DOX dose exceeds 550 mg/m^2 [2-4]. Various hypotheses have been proposed regarding the occurrence and progression mechanisms of DIC, including oxidative stress, DNA damage, autophagy, and ferroptosis [5-8]. Recent research has emphasized the crucial role of ferroptosis in the occurrence and progression of DIC [8-11].

***Corresponding author**
liwenjun@hospital.cqmu.edu.cn, liusq@hospital.cqmu.edu.cn

Received 14 February 2025
Received in revised from 6 April 2025
Accepted 12 August 2025

Ferroptosis is a form of Fe-dependent cell death characterized by abnormal intracellular accumulation of reactive oxygen species (ROS) [12, 13]. Previous studies have shown that doxorubicin can increase Fe^{2+} levels in cardiomyocytes through direct binding with Fe^{2+} and the modulation of iron metabolism-related gene expression. The accumulation of Fe^{2+} facilitates Fenton reactions, generating ROS and significantly increasing oxidative stress within cells. This oxidative stress further induces lipid peroxidation in cardiomyocytes, ultimately leading to cell death. Additionally, ROS may impair mitochondrial function, disrupting energy metabolism and ATP production, thereby exacerbating cardiomyocyte damage and death [11, 14]. Recent research has suggested that a high-iron diet significantly elevates the incidence of DIC in mice, whereas mice fed an iron-deficient diet exhibit a lower risk of developing DIC and an extended lifespan [15, 16]. Studies suggest that natural products, such as fisetin, licochalcone A, and taxifolin, can improve DIC by inhibiting ferroptosis [10, 17, 18]. Collectively, these findings underscore the feasibility of treating DIC through the modulation of ferroptosis.

Eriodictyol (ERD) [IUPAC name (2S)-2-(3,4-dihydroxyphenyl)5,7-dihydroxy-2,3-dihydrochromen-4-one], a flavonoid compound widely distributed in citrus fruits, vegetables, and some medicinal plants, has been reported to have various therapeutic effects, including anticancer, anti-ischaemic stroke, and cardioprotective effects [19-21]. Studies have shown that ERD can reduce myocardial ischaemia/reperfusion (I/R) injury by modulating the JAK2 pathway and improve myocardial cell injury by upregulating Bcl-2 expression and downregulating Bax and caspase-3 expression [22, 23]. Additionally, our previous research demonstrated that ERD can improve Alzheimer's disease by inhibiting ferroptosis [24]. However, the pharmacological effects and mechanisms of ERD in DIC are not yet clear and need further investigation.

This study aimed to elucidate the potential role of ERD in DIC. We report for the first time that ERD can alleviate DIC by selectively downregulating FABP4 to inhibit ferroptosis. Our findings may provide new insights into the development of therapeutic strategies for DIC.

2. Materials and methods

2.1. Cell culture and reagents

The H9c2 cell line derived from rat myocardial cells was procured from Zhong Qiao Xin Zhou Biotechnology Co., Ltd. (Shanghai, China). The cells were cultured at 37 ℃ in a CO_2 incubator with high-glucose Dulbecco's modified Eagle’s medium (DMEM) supplemented with 10% foetal bovine serum and 1% penicillin/streptomycin.

H9c2 cells were randomly divided into the following five treatment groups: the control group, the DOX group, the DOX+16 μM ERD group, the DOX+32 μM ERD group, and the DOX+64 μM ERD group. Previous studies have shown that exposing H9c2 cells to 1 μM doxorubicin for 24 hours can be used to establish a DIC cell model [10]. The control cells were cultured in normal medium for 48 hours, whereas the other groups were cultured for 24 hours before being treated with 1 μM DOX (Macklin, Shanghai, China).

Prior to DOX treatment, the cells in the treatment groups were pretreated with varying concentrations of ERD (purity ≥ 98%, a gift from Syntech (SSPF) International Inc., California, USA) for 2 hours.

2.2. Animals and treatments

All wild-type C57BL/6J mice (male, 6–8 weeks old) were obtained from the Animal Experimental Centre of Chongqing Medical University (Chongqing, China). The mice were housed and cared for at the Animal Experimental Centre of Chongqing Medical University. All mouse care procedures and experimental procedures in this study were approved by the Animal Ethics Committee of Chongqing Medical University (IACUC-CQMU-2023-0028). Prior to experimentation, the mice were acclimated to the laboratory environment for one week.

The mice were randomly divided into six groups (n = 5 per group): the Vehicle group, ERD group (ERD 100 mg/kg/day), DOX group, DOX+ERD-50 (ERD 50 mg/kg/day) group, DOX+ERD-100 (ERD 100 mg/kg/day) group, and DOX+DXZ group. The solvents for the aforementioned drugs consisted of 1% DMSO, 40% PEG 300, and 59% saline, and the drugs were administered to the mice via intraperitoneal injection. In accordance with previous studies, DIC animal models were established in mice via the administration of a single dose of 20 mg/kg DOX [8]. Seven days prior to DOX administration and after the injection, the mice were treated with either solvent or ERD according to their respective groups. In the DOX+DXZ group, the mice received 200 mg/kg dexrazoxane (Macklin, Shanghai, China) 30 minutes before DOX administration. Four days after the DOX injection, echocardiography was performed. The animals were subsequently euthanized, and blood samples and hearts were collected for further analysis.

2.3. Echocardiography

Following the completion of mouse dosing, the mice were lightly anaesthetized with isoflurane (provided by the Animal Research Centre of Chongqing Medical University). Portable digital colour Doppler ultrasonography (VINNO, Jiangsu, China) was employed to conduct echocardiographic assessments and evaluate mouse cardiac function. The examination focused on the short-axis view of the left ventricular papillary muscle in the heart. The cardiac function indices measured in this study included the left ventricular ejection fraction (EF) and left ventricular fractional shortening (FS).

2.4. Measurement of cardiac injury biomarkers in serum

Cardiac injury biomarkers, including creatine kinase (CK), creatine kinase-MB (CK-MB), cardiac troponin T (cTnT), and lactate dehydrogenase (LDH), were quantified in mouse serum. A Mouse CK ELISA Kit, Mouse CK-MB ELISA Kit, Mouse cTnT ELISA Kit, and Mouse LDH/LDHA ELISA Kit were used for these measurements, and the kits were obtained from Animalunion Biotechnology (Shanghai, China).

2.5. Cardiac tissue histological analysis

Mouse cardiac tissues were fixed in 4% paraformaldehyde, subsequently embedded in paraffin, and sectioned into 5 μm-thick slices. Masson staining (Beyotime, Shanghai, China) was used to assess myocardial fibrosis, whereas haematoxylin and eosin (H&E) staining (Beyotime, Shanghai, China) was used to observe

mouse myocardial structure. The stained sections were observed and imaged using an inverted fluorescence microscope (Nikon, Tokyo, Japan).

2.6. Cell viability assay

The effects of various treatments on the viability of H9c2 cardiomyocytes were assessed via a Cell Counting Kit-8 (CCK-8) assay kit (ApexBio Technology, Houston, USA). H9c2 cells were seeded at a density of 5000 cells per well in a 96-well plate. Following the completion of drug treatments, 10 μL of CCK-8 working solution was added to each well, and the cells were further incubated for 4 hours in the cell culture incubator. The optical density (OD) values at 450 nm were then measured using a microplate reader (BioTek, Vermont, USA).

2.7. Lactate dehydrogenase (LDH) assay in cell supernatants

The levels of LDH in H9c2 cells were determined using a Lactate Dehydrogenase (LDH) Cytotoxicity Assay Kit (Beyotime, Shanghai, China).

2.8. Propidium iodide (PI) staining

The effects of various treatments on H9c2 cell death were assessed via the use of a PI staining solution (Beyotime, Shanghai, China). Observation and imaging were conducted using an inverted fluorescence microscope (Nikon, Tokyo, Japan).

2.9. Detection of malondialdehyde (MDA) and iron contents

The levels of MDA were assessed in mouse cardiac tissue and H9c2 cells using the Lipid Peroxidation Product MDA Assay Kit (Beyotime, Shanghai, China). Simultaneously, the contents of Fe^{2+} and total iron (Fe) in both mouse cardiac tissue and H9c2 cells were determined using an Iron Assay Kit - Colorimetric (DOJINDO, Kumamoto, Japan).

2.10. Transmission electron microscopy

Fresh left ventricular myocardial tissue from mice, approximately 1 mm × 1 mm × 1 mm in size, was initially fixed with 3% glutaraldehyde, followed by secondary fixation with 1% osmium tetroxide. The tissue was progressively dehydrated, permeabilized, embedded, sectioned, and stained. Morphological observations of the mitochondrial structure were conducted via a JEM-1400FLASH transmission electron microscope (JEOL, Tokyo, Japan).

2.11. ROS and lipid peroxidation assays

The levels of ROS in H9c2 cardiac cells were assessed using DCFH-DA staining solution (Beyotime, Shanghai, China) and dihydroethidium (DHE) staining solution (Beyotime, Shanghai, China). H9c2 cardiac cell culture medium was aspirated, washed with PBS, and treated with a working solution of DCFH-DA (10 μM) or DHE (5 μM), which was diluted in serum-free culture medium. After 30 minutes of incubation at 37 ℃, the cells were washed with serum-free medium, observed and imaged using an inverted fluorescence microscope (Nikon, Tokyo, Japan).

2.12. Calcein AM staining

The influence of different treatments on the metal ion concentration in H9c2 cells was assessed via the use of calcein AM staining solution (Beyotime, Shanghai, China). Observation and imaging were conducted using an inverted fluorescence microscope (Nikon, Tokyo, Japan).

2.13. Western blot analysis

Total protein was extracted from tissues and cells via RIPA lysis buffer (Beyotime, Shanghai, China) containing protease and phosphatase inhibitors. The protein concentration was determined via a BCA protein concentration assay kit (Beyotime, Shanghai, China). Equal amounts of protein extracts were separated via SDS–PAGE and transferred to PVDF membranes. The membranes were blocked with QuickBlock (Beyotime, Shanghai, China) for 5–15 minutes at room temperature, followed by overnight incubation at 4 ℃ with primary antibodies against β-actin (1:10000, Bimake, Houston, USA), GPX4 (1:1000, Bimake, Houston, USA), ferritin (1:1000, Bimake, Houston, USA), ACSL4 (1:10000, Selleck, Houston, USA), FPN (1:1000; Proteintech, Wuhan, China), FSP1 (1:2000, Proteintech, Wuhan, China), xCT (1:1000; Proteintech, Wuhan, China), transferrin receptor (1:2000, Affinity Biosciences, Jiangsu, China), and FABP4 (1:500, ZEN-BIOSCIENCE, Sichuan, China). The membranes were subsequently incubated at room temperature in the dark for 2 hours with the following secondary antibodies: H&L (IRDye 800CW) secondary antibodies (1:2000, Abcam, Cambridge, UK) and anti-rabbit IgG HRP-linked secondary antibodies (1:2000; Proteintech, Wuhan, China). The membranes were subsequently scanned using the Tanon 5200 Chemiluminescence Image Analysis System (Tanon, Shanghai, China) or Odyssey® CLx Dual-Color Infrared Imaging System (LI-COR Biosciences, Nebraska, USA) [24].

2.14. Target prediction for ERD-mediated improvement in DIC by inhibiting ferroptosis

The relevant targets for ERD were obtained from multiple databases with specific filtering criteria. The sdf file and SMILES structure of ERD were obtained from PubChem database (https://pubchem.ncbi.nlm.nih.gov/) [25]. In the PharmMapper database (http://www.lilab-ecust.cn/pharmmapper/), the SDF file of ERD was imported, and the maximum number of generated conformations was set to 300 [26]. In the SwissTargetPrediction database (http://www.swisstargetprediction.ch/), the SMILES structure of ERD was imported, and the probability threshold was set to > 0 [27]. In the TCMSP database (http://tcmspw.com/), eriodictyol was searched, and the filtering criteria of DL > 0.18 and OB > 30% were applied [28]. In the TargetNet database (http://targetnet.scbdd.com/), the SMILES structure of ERD was imported, and the AUC threshold was set to > 0.7 [29]. In the Batman database (http://bionet.ncpsb.org.cn/batman-tcm/), eriodictyol was searched, and the filtering criteria of Score cutoff = 20 and Adjusted *P*-value < 0.05 were applied [30]. Ferroptosis-associated targets were sourced from the FerrDb database (http://www.zhounan.org/ferrdb/current/), whereas cardiomyopathy (CMP)-related targets were retrieved from the GeneCards database (https://www.genecards.org/), the Disgenet database (https://www.disgenet.org/home/), the OMIM database (https://www.omim.org/), the PharmGKB database (https://www.pharmgkb.org/), and the Therapeutic Target

Database (https://db.idrblab.net/ttd/) [31-36]. In these databases, "cardiomyopathy" was directly searched, and the relevant targets were then downloaded for further analysis. For all databases, only human proteins were selected as target types.

After unifying target names through the UniProt database (https://www.uniprot.org/), the online tool Draw Venn Diagram (http://bioinformatics.psb.ugent.be/webtools/Venn/) was employed to identify intersections among ERD targets, ferroptosis targets, and cardiomyopathy targets [37]. The identified common targets were imported into Cytoscape 3.10.0 software (http://www.cytoscape.org/) to visualize the "Drug-Disease-Target" network [38]. The common targets were subsequently input into the STRING database (https://string-db.org/cgi/input.pl) for protein–protein interaction (PPI) analysis [39]. The results were output in tsv format and imported into Cytoscape 3.10.0 software. Node Fill Color and Shape Size were set based on Degree unDir to create a comprehensive protein interaction network.

2.15. Molecular docking

Molecular docking was employed to assess the binding affinity between potential targets and ERD, providing insights into their stability. The protein molecular structures of potential targets were downloaded from the PDB database (https://www.rcsb.org/), whereas the structure of ERD was obtained from the PubChem database (https://pubchem.ncbi.nlm.nih.gov/) [25, 40]. The protein and ERD structures were imported into AutoDock Tools software for processing and molecular docking. The Kollman charges for proteins and Gasteiger charges for ligands were automatically assigned by AutoDock Tools, and the proteins were fully enclosed within a grid box, utilizing a global docking method for molecular docking. Docking affinities between molecules were calculated, and the results were visualized via PyMol 2.5.5 and LigPlot (https://www.ebi.ac.uk/thornton-srv/software/LigPlus/) [41].

2.16. Molecular dynamics simulation

A molecular dynamics simulation, spanning 100 ns, was conducted for the pivotal targets via Gromacs 2019.6 software. Hydrogenation of the critical targets was performed, implementing atom parameterization with the AMBER99SB-ILDN force field. The force field parameters for water molecules were set accordingly. Ligand configurations were constructed via GaussView, and their electrostatic potentials were computed. Amber parameters and coordinate files for ligands were generated via Amber Tools. Subsequently, Acpype was employed to create the GAFF force field topology file for the ligand. The box type selected for this study was cubic, with a side length that could fully contain the protein plus an additional 0.2 nm (2 Å). Following these preparations, a series of steps, including energy minimization, NVT pre–equilibration, and NPT pre–equilibration (with an equilibrium time of 0.1 ns for both), were performed. Subsequently, molecular dynamics simulations were conducted.

2.17. Cellular thermal shift assay (CETSA)

The Cellular Thermal Shift Assay (CETSA) was adapted with slight modifications based on previous studies [42]. Briefly, the cells were collected, resuspended in PBS at five times the cell weight, and sonicated

for 5 seconds at 6 kHz. The resuspended cells were then subjected to a freeze–thaw cycle by immersion in liquid nitrogen for 1 minute, followed by incubation in a 30 ℃ water bath for 1 minute. This process was repeated three times to disrupt the cell structure and release proteins into the supernatant. After centrifugation for 10 minutes (4 ℃, 12,000 r/min), the supernatant was collected. The supernatant was divided equally into two portions, with one portion treated with ERD and the other with an equal volume of DMSO. After thorough mixing, the samples were incubated at room temperature for 1 hour. Each set of supernatants was further divided into six aliquots (47, 52, 57, 62, 67, and 72 ℃), and the samples were heated for 3 minutes at the corresponding temperatures using a heating block, followed by immediate cooling on ice. After centrifugation for 10 minutes (4 ℃, 12,000 r/min), the supernatant was collected and then boiled with 5× loading buffer (Beyotime, Shanghai, China) at 100 ℃ for 8 minutes in preparation for Western blot analysis.

2.18. Real-time quantitative PCR (qPCR)

Total RNA was extracted from H9c2 cells using the Total RNA Extraction Kit (TIANGEN, Beijing, China). The extracted RNA was then reverse-transcribed into cDNA templates using the All-in-One cDNA Synthesis SuperMix kit (Monad, Suzhou, China). QPCR was performed using gene-specific primers and the 2× SYBR Green q-PCR Master Mix kit (Bimake, Houston, USA) on a QuantStudio Dx instrument (Thermo Fisher, Massachusetts, USA) to measure mRNA expression levels. Each reaction was run in triplicate, and β-actin was used for normalization. The primers used for PCR were as follows: FABP4 (forward primer) 5′-GGGACTTGGTCGTCATCCG-3′, FABP4 (reverse primer) 5′-TTTCATGACACATTCCACCACCA-3′; β-actin (forward primer) 5′-AGATCAAGATCATTGCTCCTCCT-3′, β-actin (reverse primer) 5′-ACGCAGCTCAGTAACAGTCC-3′.

2.19. Cycloheximide (CHX) chase assay

A CHX chase assay was performed to assess whether ERD can promote the degradation of FABP4. Cells were treated with 100 μg/mL CHX (Sigma-Aldrich, Shanghai, China) for 1 h were exposed to 64 μmol/L ERD or vehicle control. Subsequently, cells were collected at the indicated time points, namely, 2 h, 4 h, 6 h, 8 h, and 12 h. The protein levels of FABP4 were determined by western blot analysis.

2.20. Construction of FABP4-knockdown H9c2 cells

The FABP4 shRNA plasmid (MiaoLingBio, Hubei, China), which is equipped with green fluorescence, has a FABP4 shRNA target sequence of 5'-GGAAAGTCGACCACCATAAAG-3'. The FABP4 shRNA plasmid and NC shRNA plasmid was transfected into HEK293T cells using Lipo8000™ Transfection Reagent (Beyotime, Shanghai, China) to generate viral particles. After 48 hours of transfection, virus particles in the cell culture supernatant were filtered through a 0.45 μm membrane and used to infect H9c2 cells at 37 ℃ in the presence of HiTransG P Virus Infection Enhancer (Genechem, Shanghai, China). Puromycin (1 μg/mL) was added to select stably infected cells. The knockdown efficiency was confirmed through observation under an inverted fluorescence microscope (Nikon, Tokyo, Japan) and Western blot analysis.

2.21. Statistical analysis of data

ImageJ was used to analyse the Western blot protein bands. A two-tailed t test was used to compare data between two groups, and one-way analysis of variance was used for the analysis of multiple groups during the analysis process. GraphPad Prism 8.0.2 software was used for data analysis in this study. The results of the analysis are presented as the means ± standard deviations (means ± SDss), with statistical significance set at $P < 0.05$.

3. Results

3.1. ERD alleviates DIC in mice

The chemical structure of ERD is illustrated in Fig. 1A, and the animal grouping is depicted in Fig. 1B. The echocardiography results demonstrated a significant reduction in the EF and FS in the mice treated with DOX compared with those in the control group (Fig. 1C). The results indicated a marked increase in the levels of cardiac injury markers (including LDH, CK, CK-MB, and cTnT) in mouse serum after DOX administration (Fig. 1D-G). Additionally, the heart size and heart-to-body weight ratio of the mice in the DOX group substantially decreased (Fig. 1H). Histological examination via H&E staining revealed evident pathological damage to the tissue induced by DOX, including the disorganized arrangement of the myocardial fibres and expanded interstitial gaps (Fig. 1I). The Masson staining results indicated that DOX induced myocardial fibrosis (Fig. 1J). These results suggest that DOX can induce pronounced cardiac dysfunction in mice.

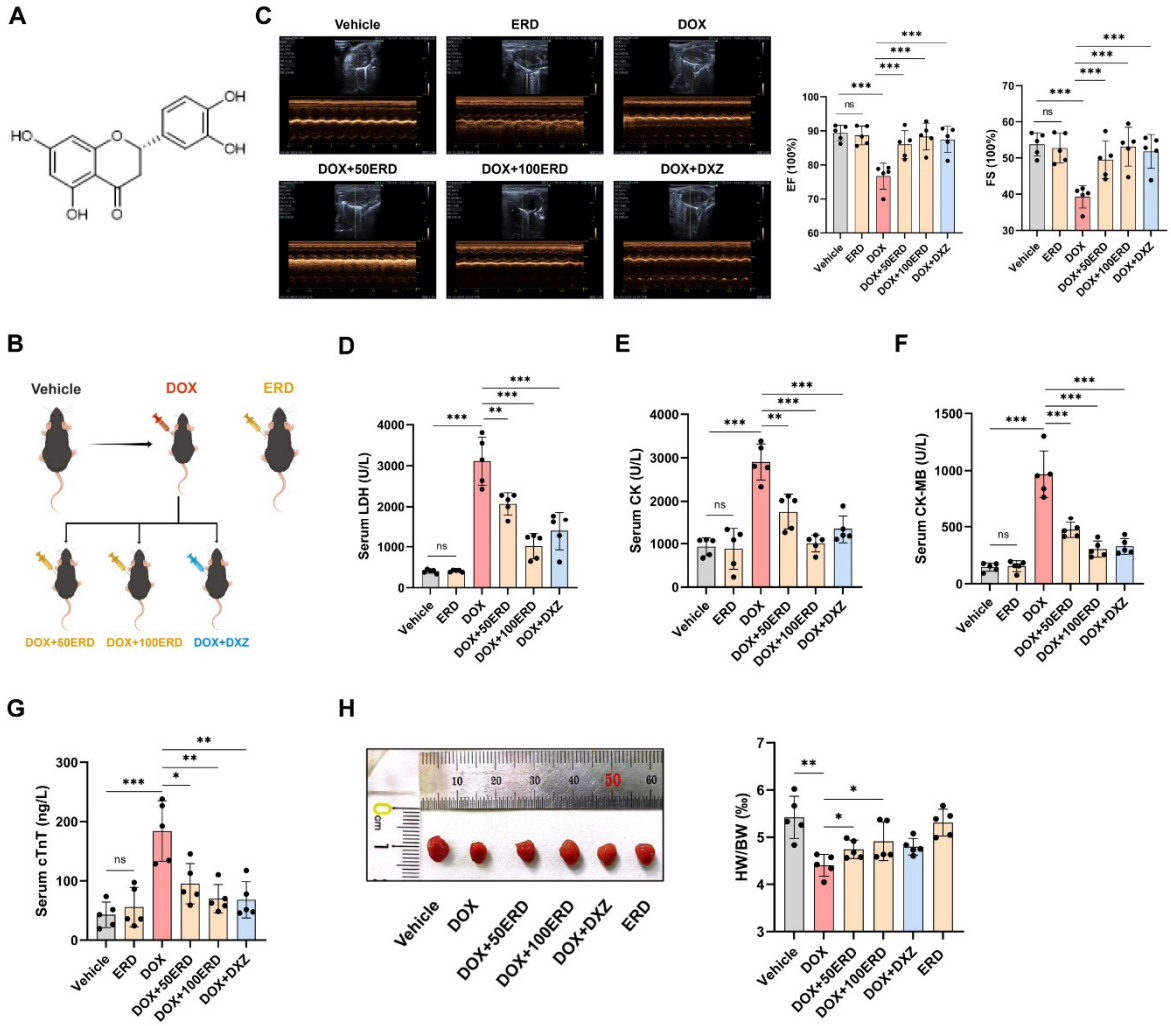

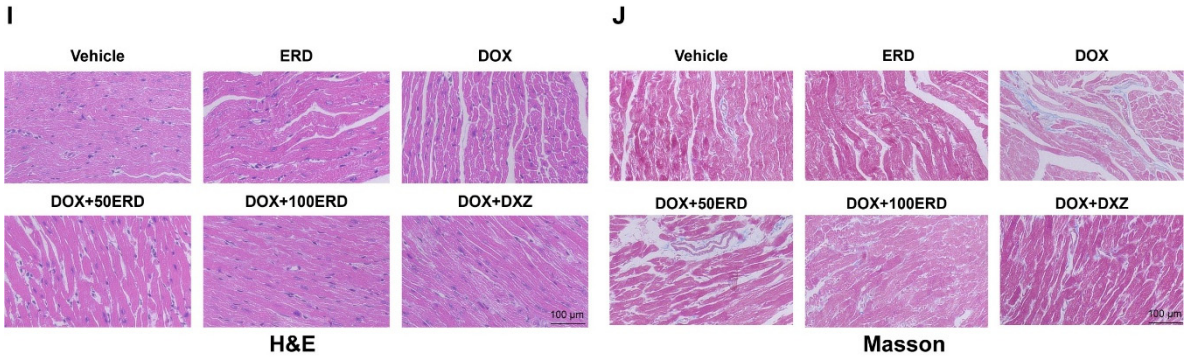

Fig. 1. ERD alleviates DOX-induced heart damage in mice. **A** Chemical structure of Eriodictyol (ERD). **B** Experimental design for evaluation of the protective effect of ERD on doxorubicin-induced cardiotoxicity (DIC) in mice (n = 5 per group). **C** Representative Echocardiography images of each group. **D-G** Levels of serum lactate dehydrogenase (LDH), creatine kinase (CK), creatine kinase-MB (CK-MB) and cardiac troponin T (cTnT). **H** Heart size and the heart-to-body weight ratio of mice. **I-J** Hematoxylin and eosin (H&E) staining and Masson staining for assessment of cardiac injury and myocardial fibrosis (Scale bar = 100 μm). The data are presented as the means ± SD of three experiments. *$P < 0.05$, **$P < 0.01$ and ***$P < 0.001$, ns (no significance).

Pretreatment with ERD alleviated DIC, as evidenced by a restored EF and FS, and reduced the serum levels of LDH, CK, CK-MB, and cTnT in the mice. Moreover, ERD pretreatment increased the heart-to-body weight ratio, reversing histopathological damage and myocardial fibrosis in mice. The protective effect of ERD, particularly at higher concentrations, resembles that of the only FDA-approved drug for the treatment of DIC, dexrazoxane (DXZ). In addition, cardiac function-related indicators did not significantly differ between the ERD monotherapy group and the control group of mice, indicating that ERD itself does not damage the heart.

3.2. ERD attenuates DOX-induced damage in H9c2 cells

The CCK-8 assay revealed that ERD at concentrations ranging from 2 to 128 μM had no cytotoxic effects on H9c2 cells (Fig. 2A). Conversely, 1.0 μM of DOX significantly reduced the viability of H9c2 cells, whereas ERD preconditioning at concentrations between 2 and 64 μM attenuated this effect (Fig. 2B). Assessment of LDH levels, a marker of cardiac injury, in H9c2 cells demonstrated that ERD reduces DOX-induced myocardial cell damage (Fig. 2C). Furthermore, the PI staining results indicated that ERD attenuated DOX-induced H9c2 cell death (Fig. 2D). These results suggest that ERD can alleviate DIC in H9c2 cells.

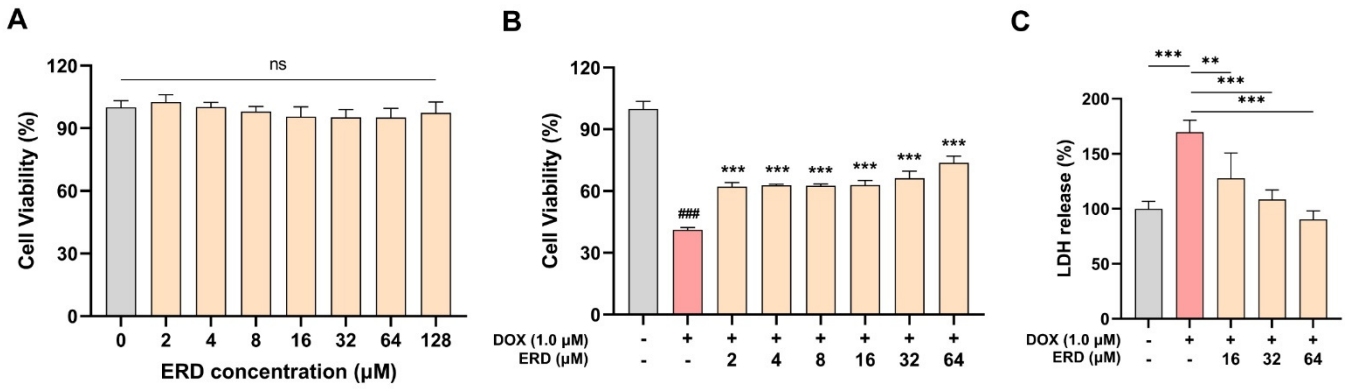

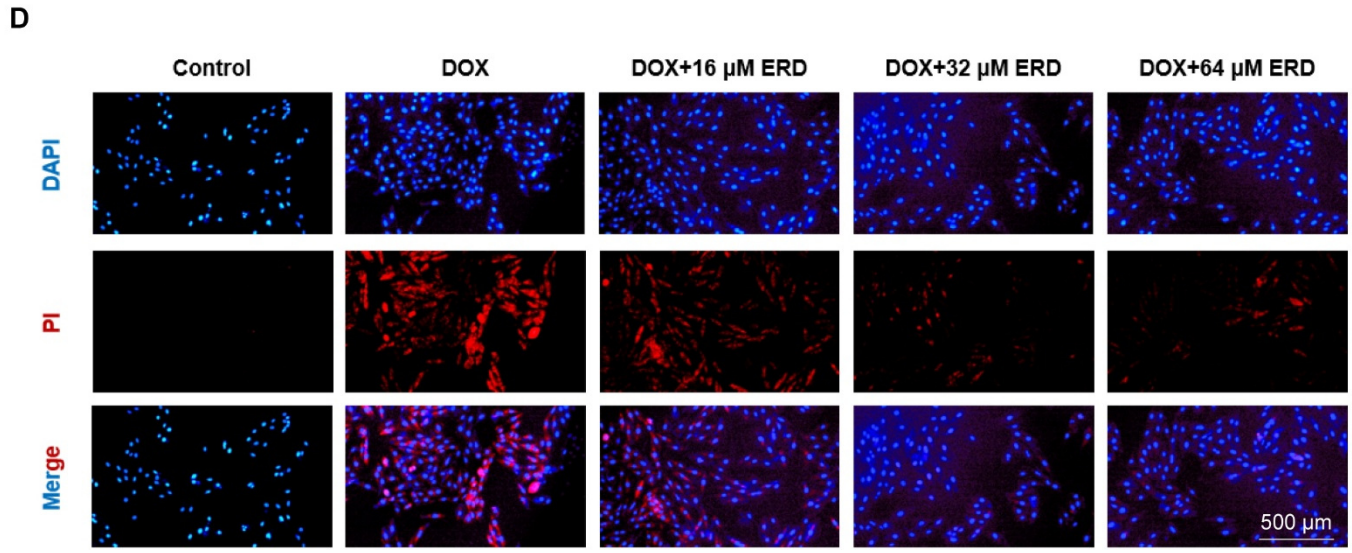

Fig. 2. ERD alleviates DOX-induced cytotoxicity in H9c2 cells. The viability of H9c2 cells were measured using a Cell Counting Kit-8 (CCK-8) assay to explore the cytotoxicity of ERD toward H9c2 cells. H9c2 cells were treated with ERD (0, 2, 4, 8, 16, 32, 64 or 128 μM) for 24 h. **A** The viability of H9c2 cells were measured using a CCK-8 assay. H9c2 cells were pre-exposed to ERD (0, 2, 4, 8, 16 or 64 μM) for 2 h and then treated with DOX (1.0 μM) for 24 h. **B** Levels of lactate dehydrogenase (LDH) of H9c2 cells. **C** Cell death was detected using DAPI and PI staining (Scale bar = 500 μm). The data are presented as the means ± SD of three experiments. $^{**}P < 0.01$ and $^{***}P < 0.001$ compared with the DOX group. $^{\#\#\#}P < 0.001$ compared with the control group, ns (no significance).

3.3. ERD reduces DOX-induced ferroptosis in mice

Ferroptosis, characterized by Fe accumulation and lipid peroxidation, represents a distinctive form of cell death and is a pivotal process in the progression of DIC [8, 12]. Selective inhibition of ferroptosis following DOX administration significantly improved cardiac function [8, 14, 43]. Our findings indicated that DOX elevated the levels of the lipid peroxidation product MDA and increased the levels of Fe^{2+} and total Fe in mouse cardiac tissue. Notably, ERD pretreatment markedly suppressed lipid peroxidation and reduced Fe^{2+} and total Fe levels (Fig. 3A-C). Additionally, we investigated the expression levels of ferroptosis-related proteins, including transferrin receptor (TfR), ferroportin (FPN), ferritin (FTH), cystine glutamate reverse transporter (xCT), ferroptosis suppressor protein 1 (FSP1), Acyl-CoA synthetase long-chain family member 4 (ACSL4) and glutathione peroxidase 4 (GPX4) [44, 45]. The Western blotting results revealed a significant increase in TfR and ACSL4 levels and substantial decreases in FPN, FTH, xCT, FSP1, and GPX4 levels in the DOX group. Importantly, ERD pretreatment effectively reduced the impact of DOX (Fig. 3D-G). Mitochondria play crucial roles in DOX-induced ferroptosis in cardiac cells [8]. Transmission electron microscopy revealed that DOX induced a notable reduction in the mitochondrial volume, an increase in the mitochondrial membrane density, and even mitochondrial rupture, whereas ERD pretreatment reversed these effects (Fig. 3H). Collectively, these results suggest that ERD can prevent DIC in mice by inhibiting ferroptosis.

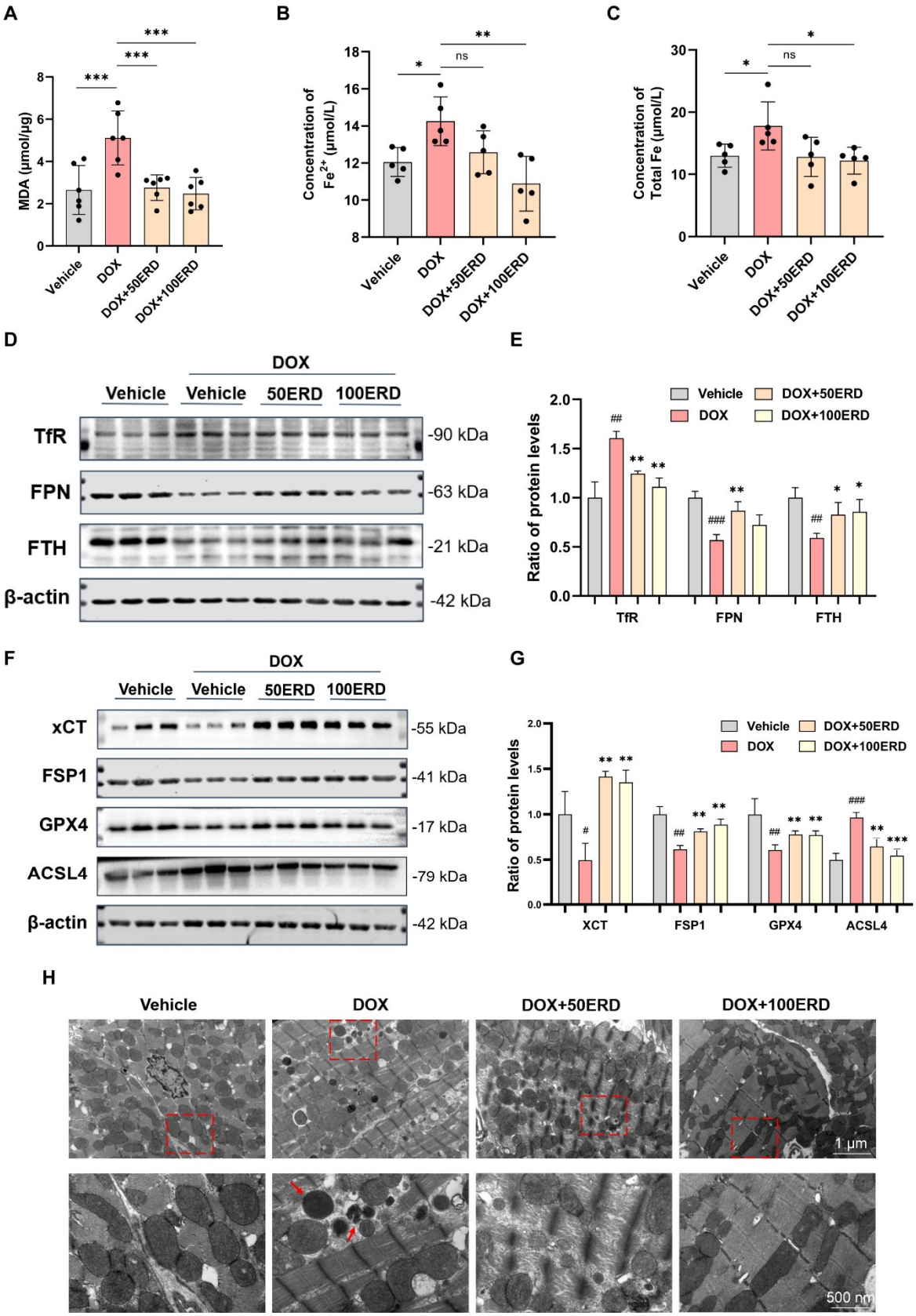

Fig. 3. ERD prevents DOX-induced ferroptosis in mouse. **A-C** Malondialdehyde (MDA) levels, Fe^{2+} levels, total Fe levels of myocardial tissue of mice. **D-G** Western blot and quantification analysis showed the expression levels of transferrin receptor (TfR), ferroportin (FPN), ferritin (FTH), cystine glutamate reverse transporter (xCT), ferroptosis suppressor protein 1 (FSP1), glutathione peroxidase 4 (GPX4) and Acyl-CoA synthetase long-chain family member 4 (ACSL4) in myocardial tissue of mice. **H** Myocardial ultrastructure of mitochondrial morphology using transmission electron microscopy (Scale bar = 1 μm or 500 nm). The data are presented as the means ± SD of three experiments. $^{*}P < 0.05$, $^{**}P < 0.01$ and $^{***}P < 0.001$ compared with the DOX group. $^{\#}P < 0.05$, $^{\#\#}P < 0.01$ and $^{\#\#\#}P < 0.001$ compared with the control group, ns (no significance).

3.4. ERD reduces DOX-induced ferroptosis in H9c2 cells

In our investigation, we explored the potential of inhibitors of ferroptosis (ferrostatin-1, Fer-1), autophagy (bafilomycin A1, BAF1), apoptosis (Z-VAD-FMK), necroptosis (necrosulfonamide, Nec), and pyroptosis inhibitor (VX-765) in attenuating DOX-induced toxicity in H9c2 cells [46-49]. Their therapeutic effects were compared with those of ERD. The CCK-8 results revealed that ERD, Fer-1, Z-VAD-FMK, and Nec prevented the toxic effects of DOX in H9c2 cells, with Fer-1 demonstrating an effect closely resembling that of ERD (Fig. 4A). Erastin and RSL3 are confirmed inducers of ferroptosis [50, 51]. Our CCK-8 results indicated that erastin (1-20 μM) and RSL3 (0.4-1.5 μM) significantly reduced H9c2 cell viability and that ERD pretreatment reduced their toxic effects on H9c2 cells (Fig. 4B-E). Our findings suggested that DOX induces lipid peroxidation and elevates ROS, Fe^{2+}, total Fe, and metal ion levels in H9c2 cells (Fig. 4F-J). Western blotting revealed a significant increase in TfR and ACSL4 levels in the DOX group, whereas FPN, FTH, xCT, GPX4, and FSP1 levels significantly decreased (Fig. 4K and L). Moreover, ERD pretreatment ameliorated the effects of DOX, mitigating lipid peroxidation and reducing ROS, Fe^{2+}, and total Fe levels in H9c2 cells. Additionally, ERD reduced the effects of DOX on ferroptosis-related proteins. In conclusion, ERD improved DIC in H9c2 cells by inhibiting ferroptosis.

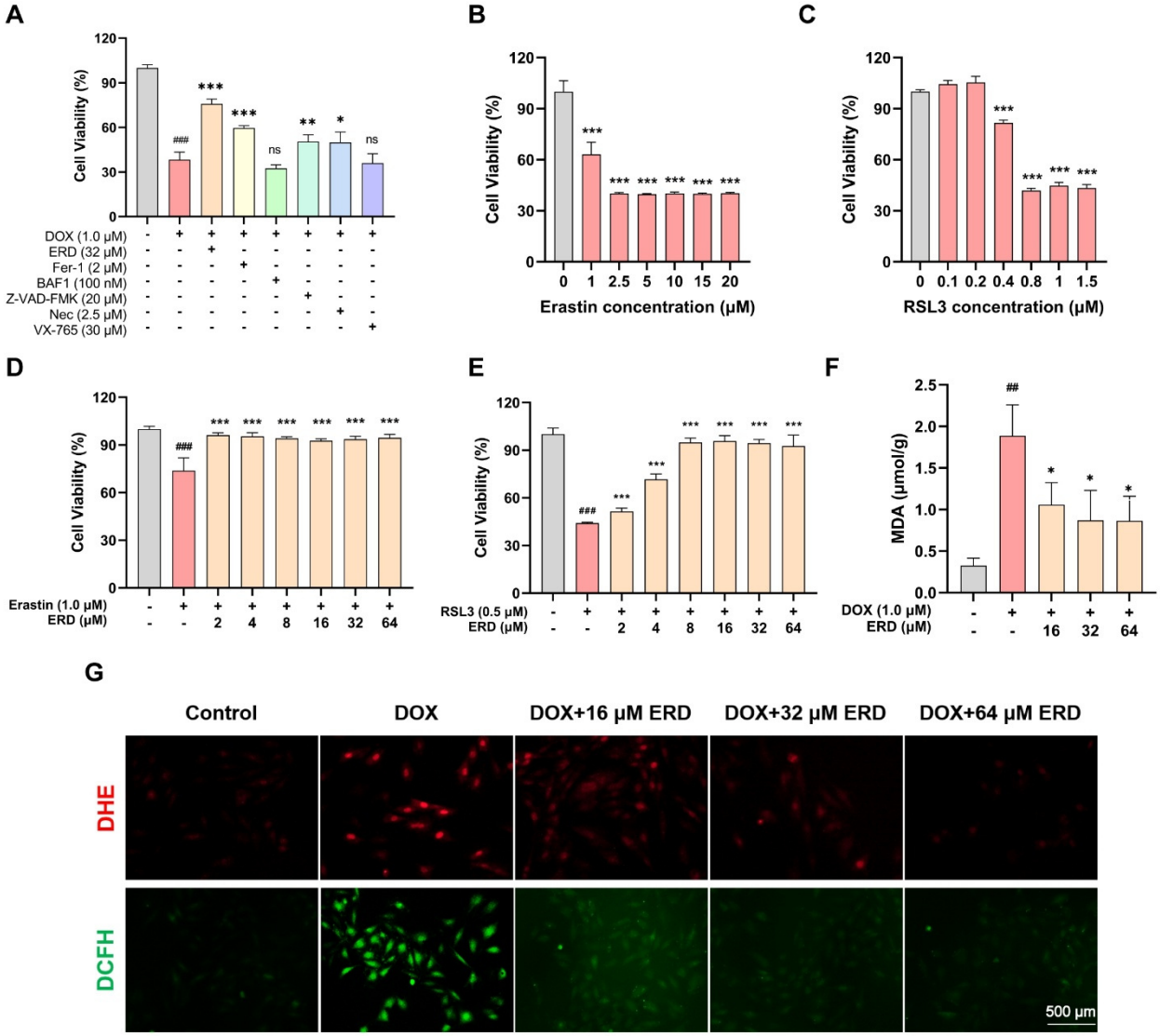

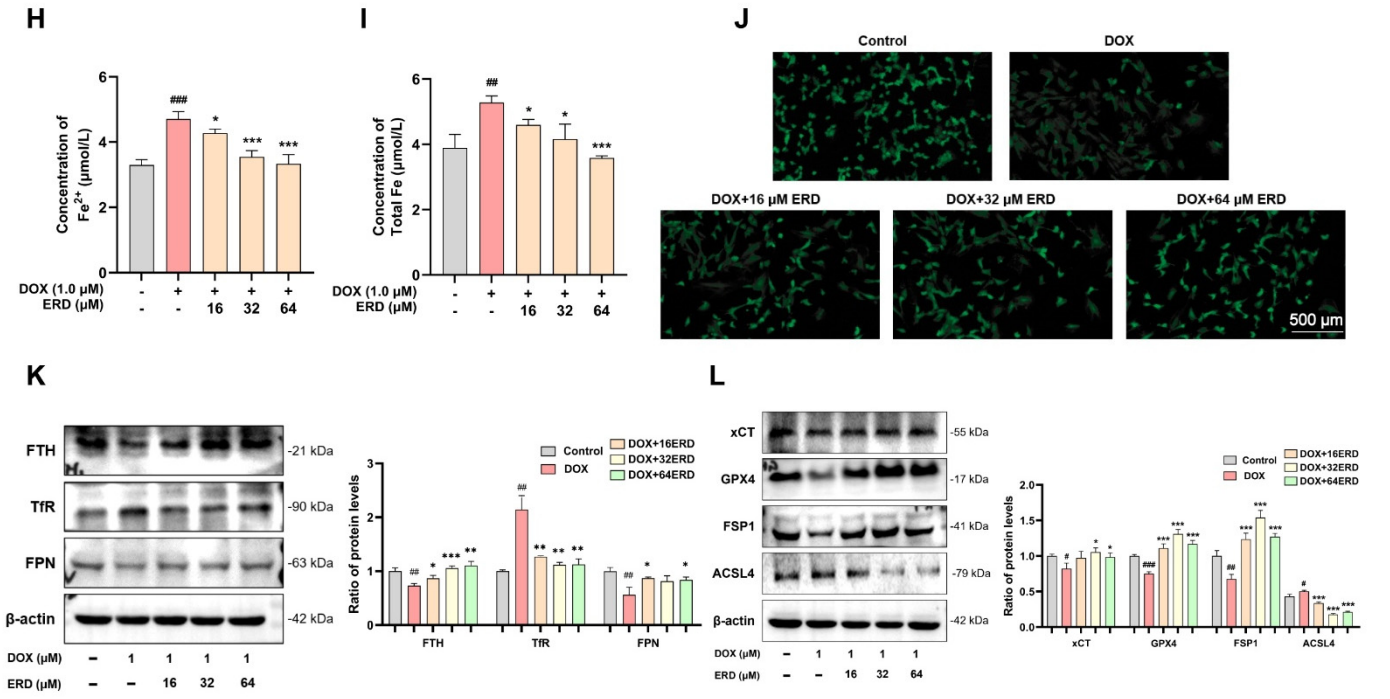

Fig. 4. ERD prevents DOX-induced ferroptosis in H9c2 cells. **A** The viability of H9c2 cells were measured using a CCK-8 assay. H9c2 cells were pre-exposed to ERD (32 μM), ferroptosis inhibitor (Ferrostatin-1, Fer-1) (2 μM), autophagy inhibitor (Bafilomycin A1, BAF1) (100 nm), apoptosis inhibitor (Z-VAD-FMK) (20 μM), necroptosis inhibitor (Necrosulfonamide, Nec) (2.5 μM), pyroptosis inhibitor (VX-765) (30 μM) for 2 h and then treated with DOX (1.0 μM) for 24 h. **B-C** The viability of H9c2 cells were measured using a CCK-8 assay to explore the cytotoxicity of Erastin and RSL3 toward H9c2 cells. H9c2 cells were treated with Erastin (0, 1, 2.5, 5, 10, 15 or 20 μM) or RSL3 (0, 0.1, 0.2, 0.4, 0.8, 1 or 1.5 μM) for 24 h. **D-E** The viability of H9c2 cells were measured using a CCK-8 assay. H9c2 cells were pre-exposed to ERD (0, 2, 4, 8, 16 or 64 μM) for 2 h and then treated with Erastin (1.0 μM) or RSL3 (0.5 μM) for 24 h. **F-J** MDA levels, ROS levels, Fe^{2+} levels, total Fe levels, metal ion levels of H9c2 cells. **K-L** Western blot and quantification analysis showed the expression levels of TfR, FPN, FTH, xCT, GPX4, FSP1 and ACSL4 in H9c2 cells. The data are presented as the means ± SD of three experiments. $^{*}P < 0.05$, $^{**}P < 0.01$ and $^{***}P < 0.001$ compared with the DOX group. $^{\#}P < 0.05$, $^{\#\#}P < 0.01$ and $^{\#\#\#}P < 0.001$ compared with the control group, ns (no significance).

3.5. FABP4 is a potential target through which ERD inhibits ferroptosis to improve DIC

A total of 349 ERD-related targets, 483 ferroptosis-related targets, and 4364 cardiomyopathy-related targets were obtained via the PharmMapper, SwissTargetPrediction, TCMSP, FerrDb, GeneCards, Disgenet, and OMIM databases (Fig. 5A). By intersecting these datasets, 18 common targets were obtained (Fig. 5A). The "Drug-Disease-Target" network diagram was constructed in Cytoscape 3.10.0 software, incorporating ERD, ferroptosis, cardiomyopathy, and the 18 common targets (Fig. 5B). The protein–protein interaction (PPI) network is illustrated in Fig. 5C. The molecular docking results revealed that ERD exhibited the lowest binding energy with FABP4 (-9.4 kcal/mol), suggesting a high affinity between ERD and FABP4 (Fig. 5D). BMS-309403, a small molecule confirmed as an inhibitor of FABP4, was used for comparison [52, 53]. Surprisingly, the binding energy of FABP4 with ERD (-9.4 kcal/mol) was even lower than that with BMS-309403 (-8.0 kcal/mol) (Fig. 5E). Compared with FABP4 alone, molecular dynamics simulations via Gromacs software revealed low root mean square deviation (RMSD) fluctuations and root mean square fluctuation (RMSF) deviations in the ERD-FABP4 complex, suggesting the stability of the ERD-FABP4 system and minimal impact of ERD on the atomic movements of FABP4 (Fig. 5F).

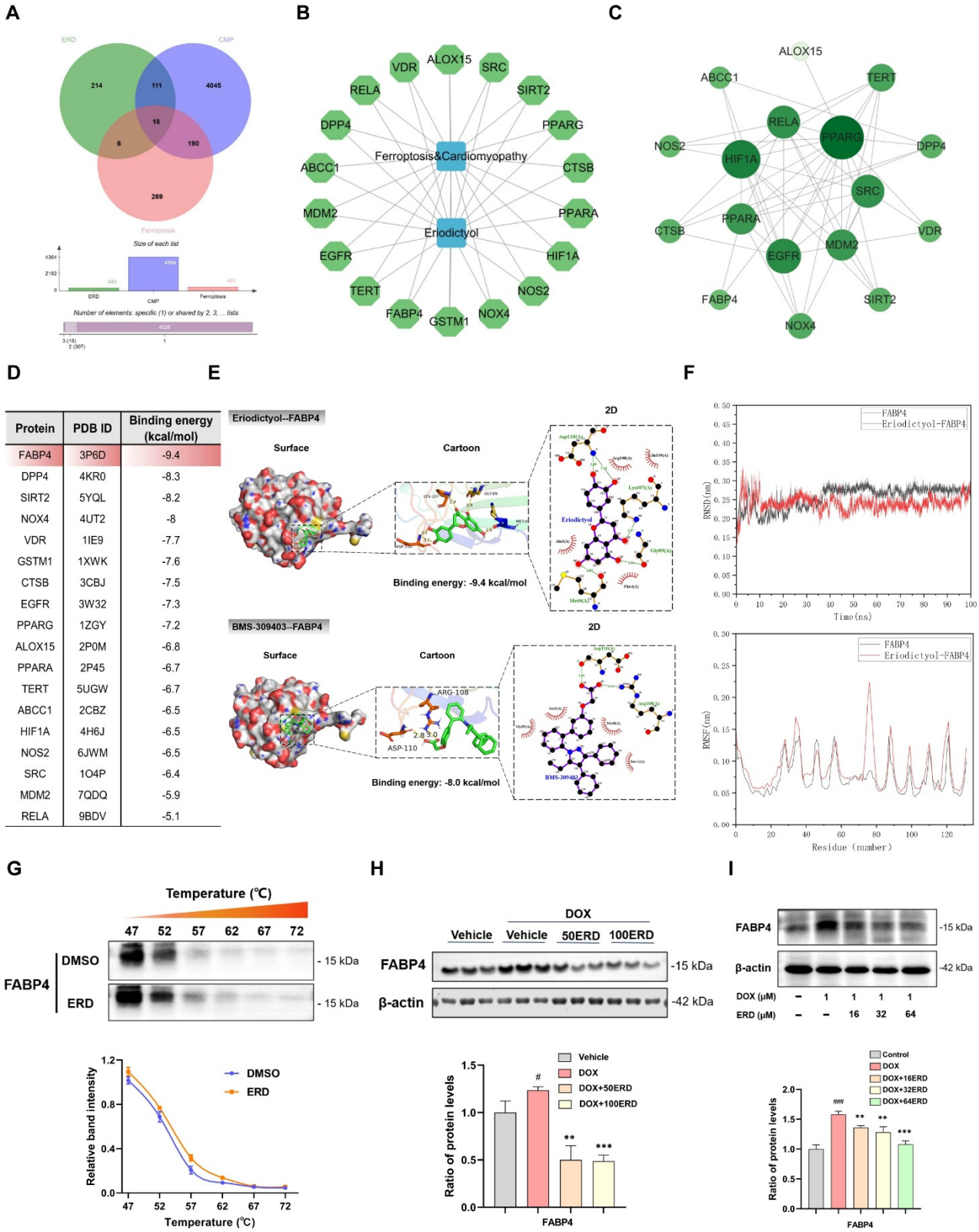

Fig. 5. ERD may inhibit ferroptosis and improve DIC by targeting and downregulating FABP4. **A** Common targets were screened via intersection by several public databases. **B-C** "Drug-Disease-Target" network and protein-protein interaction (PPI) network were mapped by Cytoscape 3.10.0 software. **D** The common targets were docked to ERD by AutoDock Tools software, and their binding affinity with ERD was evaluated based on binding energy. **E** The results of FABP4 docking with ERD and FABP4 docking with BMS-309403 were visualized using PyMol 2.5.5 and LigPlot software. **F** Molecular dynamics simulation between ERD and FABP4. **G** Cellular Thermal Shift Assay (CETSA) of FABP4 with ERD. **H-I** Western blot and quantification analysis showed the FABP4 expression levels in myocardial tissue of mice and H9c2 cells. The data are presented as the means ± SD of three experiments. $^{**}P < 0.01$ and $^{***}P < 0.001$ compared with the DOX group. $^{\#}P < 0.05$ and $^{\#\#\#}P < 0.001$ compared with the control group.

Protein	PDB ID	Binding energy (kcal/mol)
FABP4	3P6D	-9.4
DPP4	4KR0	-8.3
SIRT2	5YQL	-8.2
NOX4	4UT2	-8
VDR	1IE9	-7.7
GSTM1	1XWK	-7.6
CTSB	3CBJ	-7.5
EGFR	3W32	-7.3
PPARG	1ZGY	-7.2
ALOX15	2P0M	-6.8
PPARA	2P45	-6.7
TERT	5UGW	-6.7
ABCC1	2CBZ	-6.5
HIF1A	4H6J	-6.5
NOS2	6JWM	-6.5
SRC	1O4P	-6.4
MDM2	7QDQ	-5.9
RELA	9BDV	-5.1

Fatty acid binding protein 4 (FABP4) is an intracellular lipid chaperone, and substantial evidence supports its importance in cardiovascular diseases. It is increasingly recognized as a molecule involved in the development of cardiovascular diseases [54, 55]. Studies have also associated DOX administration with the overexpression of FABP4 [56]. Additionally, FABP4 is closely linked to ferroptosis, as evidenced by its role in the ferroptosis of HK2 and tumour cells [57, 58]. To validate the binding capacity of FABP4 with ERD, a Cellular Thermal Shift Assay (CETSA) was conducted. The CETSA demonstrated that ERD increased the thermal stability of FABP4, indicating a direct binding interaction in the cellular environment (Fig. 5G). Western blotting revealed that DOX induced an increase in FABP4 expression in mouse cardiac tissue and H9c2 cells, whereas ERD pretreatment reduced the inductive effect of DOX on FABP4 both in vitro and in vivo (Fig. 5H and I). To further investigate the mechanisms by which ERD regulates FABP4 expression levels, we performed qPCR and Cycloheximide (CHX) chase assays. The qPCR results revealed that ERD significantly attenuated the DOX-induced upregulation of FABP4 transcription; the CHX chase assay demonstrated that ERD markedly accelerated the degradation of the FABP4 protein (Supplementary Fig. 1A and B). These findings indicate that ERD downregulates FABP4 expression through a dual mechanism involving both transcriptional repression and enhanced protein degradation. In conclusion, FABP4 appears to be a promising target for ERD in the inhibition of ferroptosis to ameliorate DIC.

3.6. ERD ameliorates DIC by targeting the downregulation of FABP4 to inhibit ferroptosis

To investigate the mechanism of action, we initially knocked down FABP4 in H9c2 cells, and successful cell construction was confirmed through inverted fluorescence microscopy and Western blotting analysis (Fig. 6A). Our experiments demonstrated that ERD pretreatment alleviated the toxicity induced by DOX in normal H9c2 cells, whereas knockdown of FABP4 partially reversed the protective effect of ERD against DIC (Fig. 6B-D). ERD pretreatment reduced the elevated levels of MDA and ROS induced by DOX in normal H9c2 cells, and this effect was attenuated by FABP4 knockdown (Fig. 6E and F). Furthermore, Western blotting revealed that ERD pretreatment attenuated the increases in FABP4, TfR and ACSL4 expression and the decreases in FPN, FTH, xCT, GPX4 and FSP1 expression in DOX-treated H9c2 cells, whereas the therapeutic response of ERD was weakened with FABP4 knockdown (Fig. 6G). These data suggest that ERD exerts its inhibitory effect on ferroptosis to alleviate DIC by specifically targeting the downregulation of FABP4.

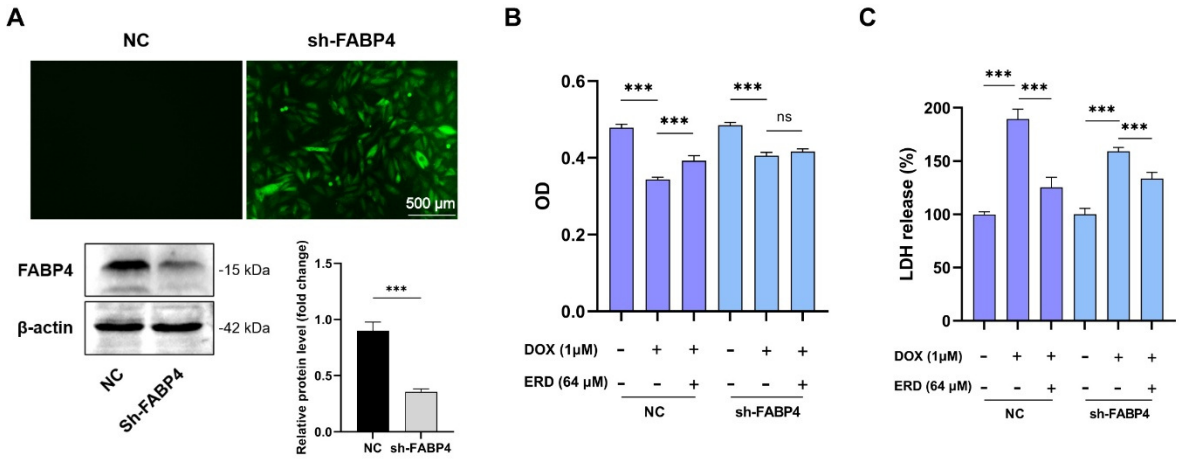

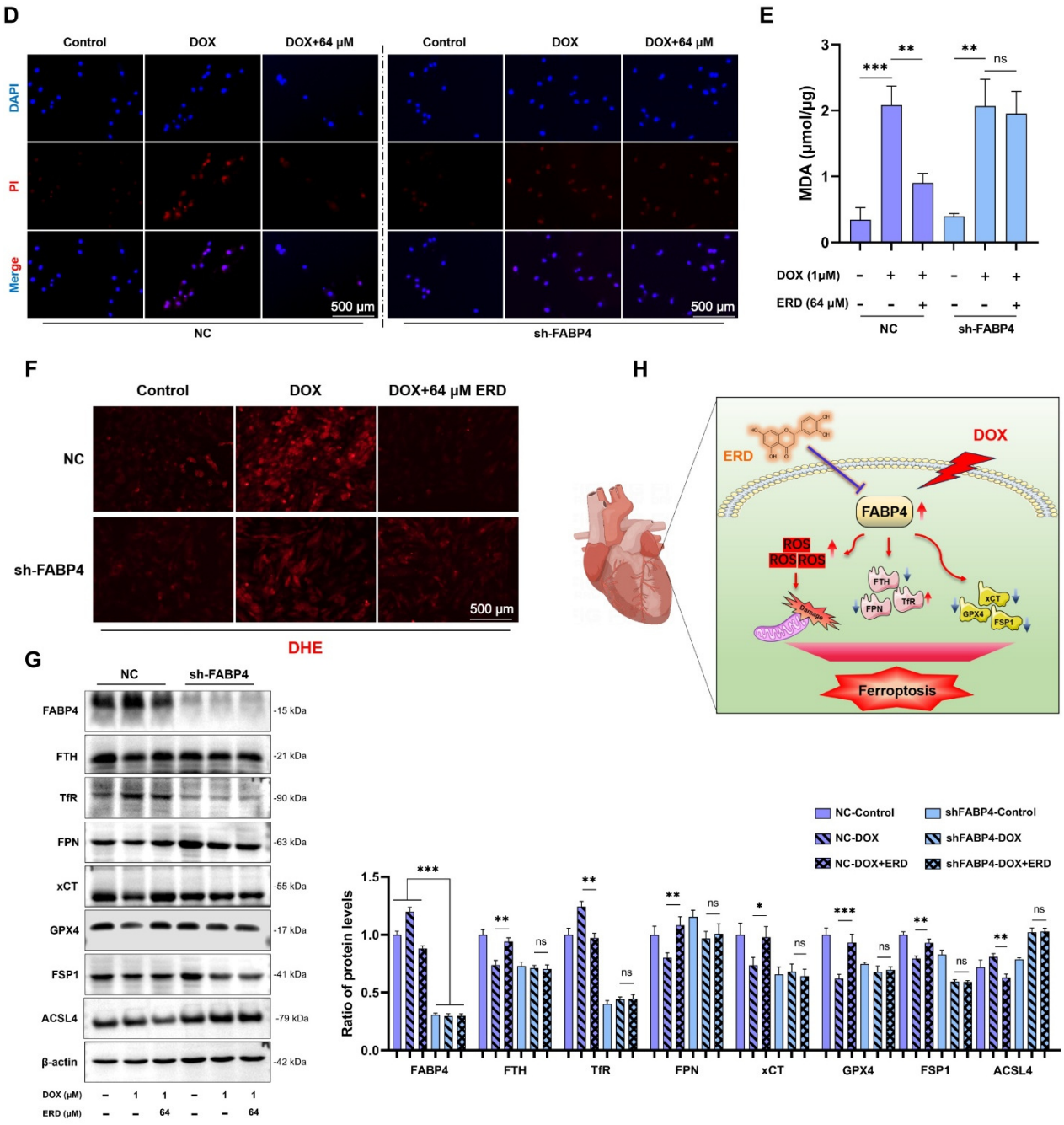

Fig. 6. FABP4 is the key target through which ERD inhibits ferroptosis to prevent DIC. **A** The green fluorescence in H9c2-shFABP4 cells was observed by inverted fluorescence microscopy (Scale bar = 500 μm), western blot and quantification analysis showed the FABP4 expression levels in H9c2-shNC and H9c2-shFABP4 cells. **B** The viability of H9c2-shNC and H9c2-shFABP4 cells were measured using a CCK-8 assay. Cells were treated with ERD (0 or 64 μM) for 2 h and then treated with DOX (1.0 μM) for 24 h. **C** Levels of lactate dehydrogenase (LDH) of cells. **D** Cell death was detected using DAPI and PI staining (Scale bar = 500 μm). **E-F** MDA levels and ROS levels of cells (Scale bar = 500 μm). **G** Western blot and quantification analysis showed the expression levels of FABP4, TfR, FPN, FTH, xCT, GPX4, FSP1 and ACSL4 in H9c2-shNC and H9c2-shFABP4 cells. **H** "ERD improves DIC by modulating FABP4 to inhibit ferroptosis" flow chart. The data are presented as the means ± SD of three experiments. *$P < 0.05$, **$P < 0.01$ and ***$P < 0.001$, ns (no significance).

4. Discussion

The sole FDA-approved drug for countering DIC, dexrazoxane (DXZ), may inhibit the antitumour effects of DOX and carry risks of haematological side effects and secondary malignancies [8, 11, 59-63]. Consequently, alternative therapeutic strategies or drugs to effectively combat DIC are urgently needed. ERD

has various biological effects, including anti-Alzheimer's disease, anticancer, anti-ischaemic stroke, and cardioprotective effects [19-21, 24]. Extensive research has confirmed that ERD exerts its cardioprotective effects through multiple pathways, such as modulation of the JAK2 pathway, activation of the Bcl-2 signalling pathway, and activation of the ERK/Nrf2/ARE pathway [21-23]. Our results indicate that ERD can improve DIC both in vitro and in vivo by inhibiting ferroptosis, with FABP4 potentially playing a crucial role in this process. Specifically, ERD was found to downregulate the expression of TfR and ACSL4 while upregulating the expression of FTH, FPN, xCT, GPX4, and FSP1. This modulation helps prevent iron metabolism dysregulation, reduce ROS levels, and alleviate lipid peroxidation and mitochondrial damage. This process appears to be associated with the direct interaction between ERD and FABP4, leading to a reduction in FABP4 protein levels.

DIC can lead to cardiomyocyte death, thereby triggering ventricular dysfunction and heart failure [64]. Consistent with previous studies, our findings also demonstrated that DOX induces cardiac dysfunction in mice, as shown in Fig. 1 [65]. This dysfunction is evidenced by decreases in the EF and FS, elevated myocardial injury markers, reduced heart size and weight, cardiac tissue pathological damage, and myocardial fibrosis. Similarly, as shown in Fig. 2, DOX also had cytotoxic effects on H9c2 cells in vitro. Interestingly, both in vivo and in vitro, ERD pretreatment yielded results comparable to those of the positive control drug DXZ, effectively mitigating DIC. Although DXZ is no longer used clinically as a preventive treatment for DIC due to its side effects, two retrospective studies have shown that DXZ can effectively prevent DIC [59, 66].

We investigated the effects of various cell death inhibitors on rescuing the DOX-induced reduction in H9c2 cell viability. As shown in Fig. 4A, the protective effect of ERD closely resembles that of Fer-1, a potent selective inhibitor of ferroptosis, suggesting that ERD may protect H9c2 cells by inhibiting ferroptosis [8]. Ferroptosis, a form of cell death characterized by the accumulation of Fe and intracellular reactive oxygen species (ROS), is closely linked to the development of DIC [8-11]. Consistent with previous studies, our results, as shown in Fig. 3 and Fig. 4, demonstrate that DOX induces ferroptosis in the heart, as evidenced by iron overload, lipid peroxidation, and mitochondrial damage [67]. Iron metabolism encompasses several key processes, including absorption, storage, and excretion. TfR plays a crucial role in cellular iron uptake, binding either to transferrin (TF) or to solute carrier family 39 member 14 (SLC39A14), to facilitate the entry of nonheme iron into cells. Excess iron is either stored in FTH or exported via FPN, the only known iron exporter [68]. Iron ions can form complexes with calcein and are hydrolysed from calcium green AM, leading to quenching of the calcein fluorescence signal. Our findings show that ERD alleviates DOX-induced iron metabolism dysregulation by modulating TfR, FTH, and FPN, reducing iron absorption and enhancing iron storage and excretion, thereby lowering ROS levels in cardiomyocytes.

At the cellular level, ferroptosis is driven primarily by the iron-dependent lipid peroxidation process. The classic pathways for inhibiting ferroptosis involve the regulation of proteins associated with lipid oxidation. xCT facilitates the uptake of cystine, promoting the synthesis of glutathione (GSH), whereas GPX4 uses GSH to reduce phospholipid hydroperoxides, thereby inhibiting lipid peroxidation. Additionally, the FSP1-CoQ10

system can suppress phospholipid peroxidation in a GSH-independent manner [68]. In contrast, ACSL4 is a key enzyme that promotes the esterification of arachidonic acid and adrenic acid into phosphatidylethanolamine in the cell membrane, thereby catalyzing the occurrence of lipid peroxidation [45]. Our results revealed that DOX upregulates ACSL4 while downregulating the expression of xCT, GPX4, and FSP1, leading to an increase in the level of MDA (a final product of lipid peroxidation) in cardiomyocytes, thereby inducing ferroptosis. These findings are consistent with those of previous studies [69, 70]. Notably, we found that ERD significantly downregulated ACSL4 while upregulating the expression of xCT, GPX4, and FSP1, effectively inhibiting DOX-induced lipid peroxidation. Moreover, we observed that ERD significantly alleviated the increased mitochondrial membrane density and membrane rupture in mouse heart tissue, which are key features of DOX-induced cytotoxicity and ferroptosis [11, 14].

To further explore the potential targets through which ERD inhibits ferroptosis to alleviate DIC, this study, as shown in Fig. 5, employed network pharmacology, molecular docking, molecular dynamics simulations, and CETSA to identify FABP4 as a potential target involved in the ERD-mediated inhibition of ferroptosis and mitigation of DIC. The involvement of FABP4 in the onset and progression of cardiovascular diseases is well established [71-75]. Studies indicate that reduced expression of FABP4 is associated with decreased serum triglycerides and a lower risk of cardiovascular diseases [71]. Additionally, the absence of FABP4 reduces the incidence of atherosclerosis in apolipoprotein E-deficient mice fed a high-fat diet [72, 73]. Furthermore, elevated FABP4 expression has been linked to left ventricular diastolic dysfunction and heart failure [74, 75]. Consistent with these findings, DOX treatment increases FABP4 expression in mouse cardiac tissue, which aligns with our results [56]. Additionally, we found that DOX increases FABP4 expression in H9c2 cells, whereas ERD inhibits the effect of DOX on FABP4 both in vitro and in vivo. These results were further supported by our qPCR and CHX chase assays, which revealed that ERD downregulates FABP4 expression through a dual mechanism involving transcriptional repression and enhanced protein degradation.

To investigate whether ERD inhibits ferroptosis and alleviates DIC by targeting FABP4, we knocked down FABP4 in H9c2 cells, as shown in Fig. 6. We observed that the therapeutic effect of ERD in mitigating DOX-induced damage to H9c2 cells was significantly reduced after FABP4 knockdown. Studies have indicated that FABP4 can induce an increase in ROS, and inhibition of FABP4 reduces ROS levels [76, 77]. Notably, the abnormal accumulation of ROS is a hallmark of ferroptosis [8]. Research has directly established a connection between FABP4 and ferroptosis. FABP4 induces ferroptosis in HK2 cells by inhibiting fatty acid β-oxidation [57]. Interestingly, after FABP4 was knocked down, the ability of ERD to reduce ROS and MDA levels was also weakened, which is consistent with the findings of previous studies. Furthermore, FABP4 gene knockout attenuated the effects of ERD in reducing the DOX-induced upregulation of TfR, ACSL4 and downregulation of FTH, FPN, xCT, GPX4, and FSP1. These findings suggest that FABP4 plays a role in modulating iron metabolism and lipid peroxidation, both of which are implicated in ferroptosis.

Flavonoids hold immense potential in alleviating DIC, with eriodictyol (ERD) emerging as a promising compound in this regard [10, 17, 18]. Our findings indicate that ERD specifically downregulates FABP4 to inhibit

ferroptosis, thereby alleviating DIC. However, the underlying mechanisms warrant further exploration: how do ERD and FABP4 interact, and how does this interaction influence ferroptosis and cardiac protection? Previous studies suggest that the ubiquitination of FABP4 induces structural fluctuations, which in turn directly affect its folding stability, although the specific mechanisms remain to be fully elucidated [78]. In colorectal cancer cells, TRIM3 suppresses FABP4-mediated metastasis by promoting its ubiquitin-dependent degradation [79]. This finding suggests that ERD may reduce FABP4 levels in cardiomyocytes through ubiquitination, contributing to its protective effect against DIC. Additionally, spectroscopic and molecular docking analyses have shown that ERD induces a conformational change in α-glucosidase through hydrophobic interactions, highlighting the potential of ERD to directly bind and induce structural alterations in proteins [80].

Based on existing studies and our experimental results, we propose that ERD downregulates FABP4 protein levels through a dual mechanism of transcriptional repression and accelerated protein degradation, thereby inhibiting iron metabolism and lipid peroxidation dysregulation in DOX-induced cardiomyocytes and reducing ferroptosis. However, the limitations of this study must be acknowledged. First, primary cardiomyocytes were not used in the experiments, and the findings from H9c2 cells consequently remain unverified in primary cells. Second, an FABP4 knockout mouse model was not established, preventing investigation of the role of FABP4 in ERD-mediated ferroptosis inhibition in transgenic animals. Finally, the specific pathway through which ERD binding to FABP4 downregulates its protein levels, along with the associated changes in upstream and downstream signalling, was not thoroughly explored in this study. We look forward to addressing these issues in future research.

5. Conclusion

Our findings demonstrated that ERD can attenuate DIC. This study further revealed that ERD achieves this effect by specifically downregulating FABP4 to inhibit ferroptosis in myocardial cells. In conclusion, this research highlights the potential of ERD as an effective ferroptosis inhibitor, with promising clinical potential and translational value. This study also provides new insights into the development of therapeutic strategies for DIC and other ferroptosis-mediated diseases.

Acknowledgments

This work was supported by the Third Affiliated Hospital of Chongqing Medical University (No. KY23046), the Natural Science Foundation of Chongqing (No. CSTB2024NSCQ-MSX0315), the Chongqing Key Specialty Construction Project in Clinical Pharmacy, and the Chongqing Yubei District Clinical Key Specialty Construction Project. We are grateful to Prof. Xiaoli Li (College of Pharmacy, Chongqing Medical University) for her technical guidance and assistance with the animal experiments.

Availability of data and materials

The data that support the findings of this study are available on request from the corresponding author.

Ethics approval and consent to participate

All mouse care procedures and experimental procedures in this study were approved by the Animal Ethics Committee of Chongqing Medical University (IACUC-CQMU-2023-0028).

Consent for publication

Not applicable.

Conflict of interest

The authors declare no conflicts of interest.

References

[1] P.K. Singal, N. Iliskovic, Doxorubicin-induced cardiomyopathy, N Engl J Med. 339 (1998) 900-5. https://doi.org/10.1056/NEJM199809243391307.

[2] P. Vejpongsa, E.T. Yeh, Prevention of anthracycline-induced cardiotoxicity: challenges and opportunities, J Am Coll Cardiol. 64 (2014) 938-45. https://doi.org/10.1016/j.jacc.2014.06.1167.

[3] W. Yu, Y. Hu, Z. Liu, et al., Sorting nexin 3 exacerbates doxorubicin-induced cardiomyopathy via regulation of TFRC-dependent ferroptosis, Acta Pharm Sin B. 13 (2023) 4875-4892. https://doi.org/10.1016/j.apsb.2023.08.016.

[4] E. Christidi, L.R. Brunham, Regulated cell death pathways in doxorubicin-induced cardiotoxicity, Cell Death Dis. 12 (2021) 339. https://doi.org/10.1038/s41419-021-03614-x.

[5] M. Songbo, H. Lang, C. Xinyong, et al., Oxidative stress injury in doxorubicin-induced cardiotoxicity, Toxicol Lett. 307 (2019) 41-48. https://doi.org/10.1016/j.toxlet.2019.02.013.

[6] W. Yu, H. Xu, Z. Sun, et al., TBC1D15 deficiency protects against doxorubicin cardiotoxicity via inhibiting DNA-PKcs cytosolic retention and DNA damage, Acta Pharm Sin B. 13 (2023) 4823-4839. https://doi.org/10.1016/j.apsb.2023.09.008.

[7] C.G. Nebigil, L. Desaubry, Updates in Anthracycline-Mediated Cardiotoxicity, Front Pharmacol. 9 (2018) 1262. https://doi.org/10.3389/fphar.2018.01262.

[8] X. Fang, H. Wang, D. Han, et al., Ferroptosis as a target for protection against cardiomyopathy, Proc Natl Acad Sci U S A. 116 (2019) 2672-2680. https://doi.org/10.1073/pnas.1821022116.

[9] Y. Wang, S. Yan, X. Liu, et al., PRMT4 promotes ferroptosis to aggravate doxorubicin-induced cardiomyopathy via inhibition of the Nrf2/GPX4 pathway, Cell Death Differ. 29 (2022) 1982-1995. https://doi.org/10.1038/s41418-022-00990-5.

[10] D. Li, X. Liu, W. Pi, et al., Fisetin Attenuates Doxorubicin-Induced Cardiomyopathy In Vivo and In Vitro by Inhibiting Ferroptosis Through SIRT1/Nrf2 Signaling Pathway Activation, Front Pharmacol. 12 (2021) 808480. https://doi.org/10.3389/fphar.2021.808480.

[11] Y. Ichikawa, M. Ghanefar, M. Bayeva, et al., Cardiotoxicity of doxorubicin is mediated through mitochondrial iron accumulation, J Clin Invest. 124 (2014) 617-30. https://doi.org/10.1172/JCI72931.

[12] S.J. Dixon, K.M. Lemberg, M.R. Lamprecht, et al., Ferroptosis: an iron-dependent form of nonapoptotic cell death, Cell. 149 (2012) 1060-72. https://doi.org/10.1016/j.cell.2012.03.042.

[13] D.R. Green, The Coming Decade of Cell Death Research: Five Riddles, Cell. 177 (2019) 1094-1107. https://doi.org/10.1016/j.cell.2019.04.024.

[14] T. Tadokoro, M. Ikeda, T. Ide, et al., Mitochondria-dependent ferroptosis plays a pivotal role in doxorubicin cardiotoxicity, JCI Insight. 5 (2020). https://doi.org/10.1172/jci.insight.132747.

[15] G.S. Panjrath, V. Patel, C.I. Valdiviezo, et al., Potentiation of Doxorubicin cardiotoxicity by iron loading in a rodent model, J Am Coll Cardiol. 49 (2007) 2457-64. https://doi.org/10.1016/j.jacc.2007.02.060.

[16] A.V. Menon, J. Kim, Iron Promotes Cardiac Doxorubicin Retention and Toxicity Through Downregulation of the Mitochondrial Exporter ABCB8, Front Pharmacol. 13 (2022) 817951. https://doi.org/10.3389/fphar.2022.817951.

[17] G. Chen, S. Luo, H. Guo, et al., Licochalcone A alleviates ferroptosis in doxorubicin-induced cardiotoxicity via the PI3K/AKT/MDM2/p53 pathway, Naunyn Schmiedebergs Arch Pharmacol. (2023). https://doi.org/10.1007/s00210-023-02863-1.

[18] Z. Lin, J. Wang, Taxifolin protects against doxorubicin-induced cardiotoxicity and ferroptosis by adjusting microRNA-200a-mediated Nrf2 signaling pathway, Heliyon. 9 (2023) e22011. https://doi.org/10.1016/j.heliyon.2023.e22011.

[19] F. Lv, Q. Du, L. Li, et al., Eriodictyol inhibits glioblastoma migration and invasion by reversing EMT via downregulation of the P38 MAPK/GSK-3beta/ZEB1 pathway, Eur J Pharmacol. 900 (2021) 174069. https://doi.org/10.1016/j.ejphar.2021.174069.

[20] S. Guo, N. Xing, G. Xiang, et al., Eriodictyol: a review of its pharmacological activities and molecular mechanisms related to ischemic stroke, Food Funct. 14 (2023) 1851-1868. https://doi.org/10.1039/d2fo03417d.

[21]A. Islam, M.S. Islam, M.K. Rahman, et al., The pharmacological and biological roles of eriodictyol, Arch Pharm Res. 43 (2020) 582-592. https://doi.org/10.1007/s12272-020-01243-0.

[22] D. Li, N. Lu, J. Han, et al., Eriodictyol Attenuates Myocardial Ischemia-Reperfusion Injury through the Activation of JAK2, Front Pharmacol. 9 (2018) 33. https://doi.org/10.3389/fphar.2018.00033.

[23] Y. Xie, R. Ji, M. Han, Eriodictyol protects H9c2 cardiomyocytes against the injury induced by hypoxia/reoxygenation by improving the dysfunction of mitochondria, Exp Ther Med. 17 (2019) 551-557. https://doi.org/10.3892/etm.2018.6918.

[24] L. Li, W.J. Li, X.R. Zheng, et al., Eriodictyol ameliorates cognitive dysfunction in APP/PS1 mice by inhibiting ferroptosis via vitamin D receptor-mediated Nrf2 activation, Mol Med. 28 (2022) 11. https://doi.org/10.1186/s10020-022-00442-3.

[25] S. Kim, J. Chen, T. Cheng, et al., PubChem 2023 update, Nucleic Acids Res. 51 (2023) D1373-D1380. https://doi.org/10.1093/nar/gkac956.

[26] X. Wang, Y. Shen, S. Wang, et al., PharmMapper 2017 update: a web server for potential drug target identification with a comprehensive target pharmacophore database, Nucleic Acids Res. 45 (2017) W356-W360. https://doi.org/10.1093/nar/gkx374.

[27] A. Daina, O. Michielin, V. Zoete, SwissTargetPrediction: updated data and new features for efficient prediction of protein targets of small molecules, Nucleic Acids Res. 47 (2019) W357-W364. https://doi.org/10.1093/nar/gkz382.

[28] J. Ru, P. Li, J. Wang, et al., TCMSP: a database of systems pharmacology for drug discovery from herbal medicines, J Cheminform. 6 (2014) 13. https://doi.org/10.1186/1758-2946-6-13.

[29] Z.J. Yao, J. Dong, Y.J. Che, et al., TargetNet: a web service for predicting potential drug-target interaction profiling via multi-target SAR models, J Comput Aided Mol Des. 30 (2016) 413-24. https://doi.org/10.1007/s10822-016-9915-2.

[30] X. Kong, C. Liu, Z. Zhang, et al., BATMAN-TCM 2.0: an enhanced integrative database for known and predicted interactions between traditional Chinese medicine ingredients and target proteins, Nucleic Acids Res. (2023). https://doi.org/10.1093/nar/gkad926.

[31] N. Zhou, X. Yuan, Q. Du, et al., FerrDb V2: update of the manually curated database of ferroptosis regulators and ferroptosis-disease associations, Nucleic Acids Res. 51 (2023) D571-D582. https://doi.org/10.1093/nar/gkac935.

[32] G. Stelzer, N. Rosen, I. Plaschkes, et al., The GeneCards Suite: From Gene Data Mining to Disease Genome Sequence Analyses, Curr Protoc Bioinformatics. 54 (2016) 1.30.1-1.30.33. https://doi.org/10.1002/cpbi.5.

[33] J. Pinero, J.M. Ramirez-Anguita, J. Sauch-Pitarch, et al., The DisGeNET knowledge platform for disease genomics: 2019 update, Nucleic Acids Res. 48 (2020) D845-D855. https://doi.org/10.1093/nar/gkz1021.

[34] J.S. Amberger, C.A. Bocchini, A.F. Scott, et al., OMIM.org: leveraging knowledge across phenotype-gene relationships, Nucleic Acids Res. 47 (2019) D1038-D1043. https://doi.org/10.1093/nar/gky1151.

[35] M. Whirl-Carrillo, R. Huddart, L. Gong, et al., An Evidence-Based Framework for Evaluating Pharmacogenomics Knowledge for Personalized Medicine, Clin Pharmacol Ther. 110 (2021) 563-572. https://doi.org/10.1002/cpt.2350.

[36] Y. Zhou, Y. Zhang, D. Zhao, et al., TTD: Therapeutic Target Database describing target druggability information, Nucleic Acids Res. 52 (2024) D1465-D1477. https://doi.org/10.1093/nar/gkad751.

[37] C. UniProt, UniProt: the Universal Protein Knowledgebase in 2023, Nucleic Acids Res. 51 (2023) D523-D531. https://doi.org/10.1093/nar/gkac1052.

[38] P. Shannon, A. Markiel, O. Ozier, et al., Cytoscape: a software environment for integrated models of biomolecular interaction networks, Genome Res. 13 (2003) 2498-504. https://doi.org/10.1101/gr.1239303.

[39] D. Szklarczyk, A. Franceschini, S. Wyder, et al., STRING v10: protein-protein interaction networks, integrated over the tree of life, Nucleic Acids Res. 43 (2015) D447-52. https://doi.org/10.1093/nar/gku1003.

[40] H.M. Berman, J. Westbrook, Z. Feng, et al., The Protein Data Bank, Nucleic Acids Res. 28 (2000) 235-42. https://doi.org/10.1093/nar/28.1.235.

[41] A.C. Wallace, R.A. Laskowski, J.M. Thornton, LIGPLOT: a program to generate schematic diagrams of protein-ligand interactions, Protein Eng. 8 (1995) 127-34. https://doi.org/10.1093/protein/8.2.127.

[42] X. Wang, C. Lin, S. Jin, et al., Cannabidiol alleviates neuroinflammation and attenuates neuropathic pain via targeting FKBP5, Brain Behav Immun. 111 (2023) 365-375. https://doi.org/10.1016/j.bbi.2023.05.008.

[43] X. Fang, Z. Cai, H. Wang, et al., Loss of Cardiac Ferritin H Facilitates Cardiomyopathy via Slc7a11-Mediated Ferroptosis, Circ Res. 127 (2020) 486-501. https://doi.org/10.1161/CIRCRESAHA.120.316509.

[44] Y. Yang, X. Wang, A. Xiao, et al., Ketogenic diet prevents chronic sleep deprivation-induced Alzheimer's disease by inhibiting iron dyshomeostasis and promoting repair via Sirt1/Nrf2 pathway, Front Aging Neurosci. 14 (2022) 998292. https://doi.org/10.3389/fnagi.2022.998292.

[45] L. Du, H. Yang, Y. Ren, et al., Inhibition of LSD1 induces ferroptosis through the ATF4-xCT pathway and shows enhanced anti-tumor effects with ferroptosis inducers in NSCLC, Cell Death Dis. 14 (2023) 716. https://doi.org/10.1038/s41419-023-06238-5.

[46] W. Fu, L. Xu, Y. Chen, et al., Luteolin induces ferroptosis in prostate cancer cells by promoting TFEB nuclear translocation and increasing ferritinophagy, Prostate. (2023). https://doi.org/10.1002/pros.24642.

[47] L. Zheng, R. Mao, X. Liang, et al., Carbon black nanoparticles and cadmium co-exposure aggravates bronchial epithelial cells inflammation via autophagy-lysosome pathway, Environ Res. 242 (2023) 117733. https://doi.org/10.1016/j.envres.2023.117733.

[48] X.Y. Zhou, B. Lin, W. Chen, et al., The brain protection of MLKL inhibitor necrosulfonamide against focal ischemia/reperfusion injury associating with blocking the nucleus and nuclear envelope translocation of MLKL and RIP3K, Front Pharmacol. 14 (2023) 1157054. https://doi.org/10.3389/fphar.2023.1157054.

[49] Y. Ji, Y. Ma, Y. Ma, et al., Rutin prevents pyroptosis and M1 microglia via Nrf2/Mac-1/caspase-1-mediated inflammasome axis to improve POCD, Int Immunopharmacol. 127 (2023) 111290. https://doi.org/10.1016/j.intimp.2023.111290.

[50] X. Chen, R. Kang, G. Kroemer, et al., Broadening horizons: the role of ferroptosis in cancer, Nat Rev Clin Oncol. 18 (2021) 280-296. https://doi.org/10.1038/s41571-020-00462-0.

[51] B. Zhou, J. Liu, R. Kang, et al., Ferroptosis is a type of autophagy-dependent cell death, Semin Cancer Biol. 66 (2020) 89-100. https://doi.org/10.1016/j.semcancer.2019.03.002.

[52] A. Mukherjee, C.Y. Chiang, H.A. Daifotis, et al., Adipocyte-Induced FABP4 Expression in Ovarian Cancer Cells Promotes Metastasis and Mediates Carboplatin Resistance, Cancer Res. 80 (2020) 1748-1761. https://doi.org/10.1158/0008-5472.CAN-19-1999.

[53] L.T. Huang, H.C. Chou, C.M. Chen, Inhibition of FABP4 attenuates hyperoxia-induced lung injury and fibrosis via inhibiting TGF-beta signaling in neonatal rats, J Cell Physiol. 237 (2022) 1509-1520. https://doi.org/10.1002/jcp.30622.

[54] Y. Umbarawan, R. Kawakami, M. Syamsunarno, et al., Reduced fatty acid uptake aggravates cardiac contractile dysfunction in streptozotocin-induced diabetic cardiomyopathy, Sci Rep. 10 (2020) 20809. https://doi.org/10.1038/s41598-020-77895-1.

[55] R. Rodriguez-Calvo, J. Girona, M. Rodriguez, et al., Fatty acid binding protein 4 (FABP4) as a potential biomarker reflecting myocardial lipid storage in type 2 diabetes, Metabolism. 96 (2019) 12-21. https://doi.org/10.1016/j.metabol.2019.04.007.

[56] L. da Cunha Menezes Souza, F.H. Fernandes, P.T. Presti, et al., Effect of doxorubicin on cardiac lipid metabolism-related transcriptome and the protective activity of Alda-1, Eur J Pharmacol. 898 (2021) 173955. https://doi.org/10.1016/j.ejphar.2021.173955.

[57] J. Chen, K. Wu, Y. Lei, et al., Inhibition of Fatty Acid beta-Oxidation by Fatty Acid Binding Protein 4 Induces Ferroptosis in HK2 Cells Under High Glucose Conditions, Endocrinol Metab (Seoul). 38 (2023) 226-244. https://doi.org/10.3803/EnM.2022.1604.

[58] G. Luis, A. Godfroid, S. Nishiumi, et al., Tumor resistance to ferroptosis driven by Stearoyl-CoA Desaturase-1 (SCD1) in cancer cells and Fatty Acid Biding Protein-4 (FABP4) in tumor microenvironment promote tumor recurrence, Redox Biol. 43 (2021) 102006. https://doi.org/10.1016/j.redox.2021.102006.

[59] R.S. Cvetkovic, L.J. Scott, Dexrazoxane : a review of its use for cardioprotection during anthracycline chemotherapy, Drugs. 65 (2005) 1005-24. https://doi.org/10.2165/00003495-200565070-00008.

[60] A.J. Wang, J. Zhang, M. Xiao, et al., Molecular mechanisms of doxorubicin-induced cardiotoxicity: novel roles of sirtuin 1-mediated signaling pathways, Cell Mol Life Sci. 78 (2021) 3105-3125. https://doi.org/10.1007/s00018-020-03729-y.

[61] P. Vejpongsa, E.T. Yeh, Topoisomerase 2beta: a promising molecular target for primary prevention of anthracycline-induced cardiotoxicity, Clin Pharmacol Ther. 95 (2014) 45-52. https://doi.org/10.1038/clpt.2013.201.

[62] E. Tahover, A. Segal, R. Isacson, et al., Dexrazoxane added to doxorubicin-based adjuvant chemotherapy of breast cancer: a retrospective cohort study with a comparative analysis of toxicity and survival, Anticancer Drugs. 28 (2017) 787-794. https://doi.org/10.1097/CAD.0000000000000514.

[63] C.K. Tebbi, W.B. London, D. Friedman, et al., Dexrazoxane-associated risk for acute myeloid leukemia/myelodysplastic syndrome and other secondary malignancies in pediatric Hodgkin's disease, J Clin Oncol. 25 (2007) 493-500. https://doi.org/10.1200/JCO.2005.02.3879.

[64] K.T. Sawicki, V. Sala, L. Prever, et al., Preventing and Treating Anthracycline Cardiotoxicity: New Insights, Annu Rev Pharmacol Toxicol. 61 (2021) 309-332. https://doi.org/10.1146/annurev-pharmtox-030620-104842.

[65] H. Chen, J. Zhu, Y. Le, et al., Salidroside inhibits doxorubicin-induced cardiomyopathy by modulating a ferroptosis-dependent pathway, Phytomedicine. 99 (2022) 153964. https://doi.org/10.1016/j.phymed.2022.153964.

[66] E.J. Chow, S. Aggarwal, D.R. Doody, et al., Dexrazoxane and Long-Term Heart Function in Survivors of Childhood Cancer, J Clin Oncol. 41 (2023) 2248-2257. https://doi.org/10.1200/JCO.22.02423.

[67] X. Zhu, X. Wang, B. Zhu, et al., Disruption of histamine/H(1)R-STAT3-SLC7A11 axis exacerbates doxorubicin-induced cardiac ferroptosis, Free Radic Biol Med. 192 (2022) 98-114. https://doi.org/10.1016/j.freeradbiomed.2022.09.012.

[68] X. Fang, H. Ardehali, J. Min, et al., The molecular and metabolic landscape of iron and ferroptosis in cardiovascular disease, Nat Rev Cardiol. 20 (2023) 7-23. https://doi.org/10.1038/s41569-022-00735-4.

[69] H. Zhang, J. Pan, S. Huang, et al., Hydrogen sulfide protects cardiomyocytes from doxorubicin-induced ferroptosis through the SLC7A11/GSH/GPx4 pathway by Keap1 S-sulfhydration and Nrf2 activation, Redox Biol. 70 (2024) 103066. https://doi.org/10.1016/j.redox.2024.103066.

[70] H. Qiu, S. Huang, Y. Liu, et al., Idebenone alleviates doxorubicin-induced cardiotoxicity by stabilizing FSP1 to inhibit ferroptosis, Acta Pharmaceutica Sinica B. (2024). https://doi.org/10.1016/j.apsb.2024.03.015.

[71] G. Tuncman, E. Erbay, X. Hom, et al., A genetic variant at the fatty acid-binding protein aP2 locus reduces the risk for hypertriglyceridemia, type 2 diabetes, and cardiovascular disease, Proc Natl Acad Sci U S A. 103 (2006) 6970-5. https://doi.org/10.1073/pnas.0602178103.

[72] L. Makowski, J.B. Boord, K. Maeda, et al., Lack of macrophage fatty-acid-binding protein aP2 protects mice deficient in apolipoprotein E against atherosclerosis, Nat Med. 7 (2001) 699-705. https://doi.org/10.1038/89076.

[73] J.B. Boord, K. Maeda, L. Makowski, et al., Combined adipocyte-macrophage fatty acid-binding protein deficiency improves metabolism, atherosclerosis, and survival in apolipoprotein E-deficient mice, Circulation. 110 (2004) 1492-8. https://doi.org/10.1161/01.CIR.0000141735.13202.B6.

[74] T. Fuseya, M. Furuhashi, S. Yuda, et al., Elevation of circulating fatty acid-binding protein 4 is independently associated with left ventricular diastolic dysfunction in a general population, Cardiovasc Diabetol. 13 (2014) 126. https://doi.org/10.1186/s12933-014-0126-7.

[75] C.L. Huang, Y.W. Wu, C.C. Wu, et al., Association between serum adipocyte fatty-acid binding protein concentrations, left ventricular function and myocardial perfusion abnormalities in patients with coronary artery disease, Cardiovasc Diabetol. 12 (2013) 105. https://doi.org/10.1186/1475-2840-12-105.

[76] G. Wu, L. Yang, Y. Xu, et al., FABP4 induces asthmatic airway epithelial barrier dysfunction via ROS-activated FoxM1, Biochem Biophys Res Commun. 495 (2018) 1432-1439. https://doi.org/10.1016/j.bbrc.2017.11.106.

[77] Y. Gong, Z. Yu, Y. Gao, et al., FABP4 inhibitors suppress inflammation and oxidative stress in murine and cell models of acute lung injury, Biochem Biophys Res Commun. 496 (2018) 1115-1121. https://doi.org/10.1016/j.bbrc.2018.01.150.

[78] D. Morimoto, E. Walinda, H. Fukada, et al., Ubiquitylation Directly Induces Fold Destabilization of Proteins, Sci Rep. 6 (2016) 39453. https://doi.org/10.1038/srep39453.

[79] Q. Zuo, Q. Xu, Z. Li, et al., TRIM3 inhibits colorectal cancer cell migration and lipid droplet formation by promoting FABP4 degradation, Histol Histopathol. 39 (2024) 239-250. https://doi.org/10.14670/HH-18-627.

[80] J.L. Liu, Y.C. Kong, J.Y. Miao, et al., Spectroscopy and molecular docking analysis reveal structural specificity of flavonoids in the inhibition of alpha-glucosidase activity, Int J Biol Macromol. 152 (2020) 981-989. https://doi.org/10.1016/j.ijbiomac.2019.10.184.